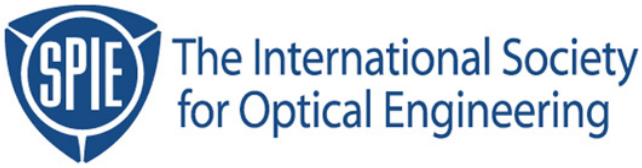

This paper was published in the proceedings of the
19th Annual BACUS Symposium on Photomask Technology and Management
SPIE Vol. 3873, pp. 2-20.
It is made available as an electronic reprint with permission of SPIE.

Electron-beam lithography simulation for maskmaking, part V: Impact of GHOST proximity effect correction on process window

Chris A. Mack
FINLE Technologies
8834 Capital of Texas Highway North, Suite 301, Austin, Texas 78759
chris_mack@finle.com

Charles Sauer
Etec Systems Inc.
26460 Corporate Avenue, Hayward, California 94545

ABSTRACT

As the requirements for photomask linewidth control continue to tighten, the necessity for performing proximity correction for electron beam mask exposure will increase. GHOST proximity effect correction is one method that can be used to ensure that critical dimension linearity over a large range of feature sizes meets mask user requirements. The GHOST strategy uses an additional exposure to correct for the backscatter component of the primary exposure. Because of the way the image using a GHOST correction is constructed, image contrast will be lower than exposures done without GHOST. This paper uses simulation to examine the process window that is available when GHOST is used and this process window is compared to that without GHOST. The effect of resist contrast on the process window is examined by simulating ZEP 7000 resist and comparing it to resists with other contrasts. The effects of dose, develop time, data bias and spot size on the process window are also examined.

Keywords: e-beam lithography, GHOST, ProBEAM/3D, ProDRM, MEBES, lithography modeling

1. Introduction

The subject of proximity effect correction for electron beam exposure systems has had a long history in the industry. More than 200 papers in the literature address this phenomenon. One of the computationally simplest systems for correcting proximity effects as applied to maskmaking is a technique called GHOST, invented by Owens and Rissman[1] more than 15 years ago. However, because of the low contrast resist systems used in maskmaking at the time, the use of this technique has never been popular. Recently, higher contrast processes have been introduced[2,3] that make the use of GHOST more attractive. In addition, the continuing reduction in feature sizes has made correcting for proximity effects necessary as a near term requirement for maskmaking. Because of how the compensating exposure for backscatter is made, most processes that use GHOST suffer from a decrease in the size of the process window compared to processes that do not use GHOST. This paper examines why a reduced process window can occur and what can be done to minimize its impact on linewidth control.

2. Basics Of Ghost Proximity Effect Correction

All electron beam lithography exposure systems exhibit proximity effects. The proximity effect is a function of backscattered electrons, which can provide additional exposure to near-by features depending on how close or proximate one feature is to another. The amount of proximity effect depends primarily on the accelerating voltage, the substrate, the resist and process, and most importantly, the size and location of the features being written.

Figure 1 shows pictorially how GHOST works. An initial exposure of the desired pattern produces an energy distribution in the resist (Figure 1a). The bar over the plot shows the pattern being exposed where white is the exposure area and black is not exposed. Note that scattering from the large spaces (clear areas) to either side of the small line (dark area) at the right of the pattern produces an overall higher energy level for this isolated line that for the small isolated space on the left side of the pattern. If one assumed a particular energy threshold level at which the resist would respond to form the final resist pattern, any one energy level would produce a linewidth that varied considerably with the density of other nearby features.

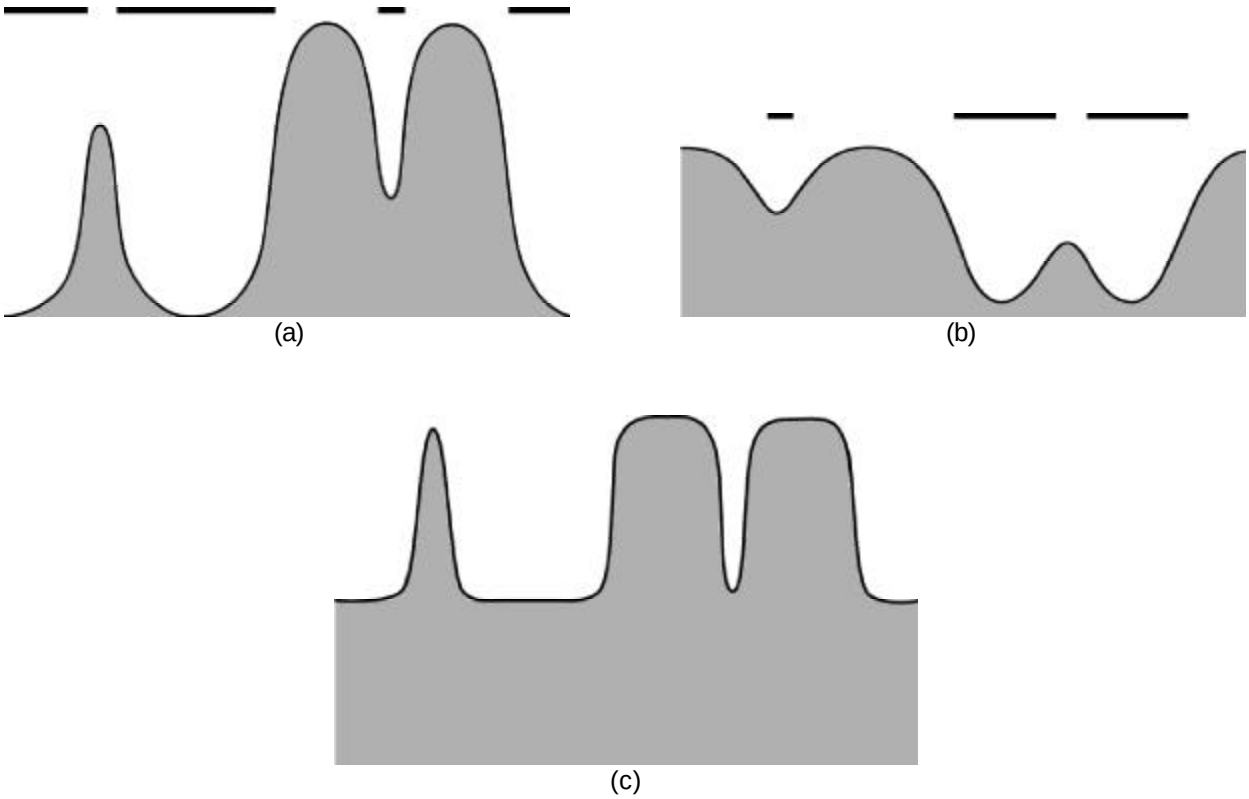

Figure 1. Image plots of exposure energy (y-axis) versus position. The combination of (a) the primary exposure plus (b) the ghost exposure produces (c) the total exposure.

If the complement of the primary exposure pattern is taken, and a reduced dose is used with a substantially larger spot size than the primary exposure, a resultant GHOST exposure is formed as seen in Figure 1b. The net result, or the addition of the two exposures, is illustrated in Figure 1c. Several things can be noted in Figure 1c. There exists an image threshold value where the isolated space (left side) has the same width as the isolated line (right side). Also, the threshold for the process is substantially different (higher) than that for just the primary exposure. Because all areas of the mask receive at least some exposure, the process latitude of the patterns are affected. In addition, with the use of GHOST exposure, resist loss for this process is higher than a process without GHOST, since the nominally unexposed areas receive some exposure. Finally, and perhaps most importantly, the primary + GHOST exposure has degraded image quality relative to the primary image alone. Actually, GHOST serves to reduce all features to the same level of image quality as an isolated dark pattern - a least common denominator approach to lithography. This situation is in some ways analogous to the use of scattering bars in wafer lithography, where isolated features are made to behave like dense features in order to

reduce the optical proximity effects. Matching a process to this GHOST writing strategy is the primary challenge to making GHOST work successfully in a manufacturing environment.

3. Dissolution Properties of Resists

Different resists can vary dramatically in their response when exposed in an electron beam exposure system. In addition, the use of GHOST, while effective in correcting proximity effects, impacts the process window differently from one resist to another. How these differences can affect lithography is the subject of this paper. The basics of determining dissolution parameters and how they can predict lithographic performance have been detailed previously[4,5]. The work described in this paper follows an earlier paper that examined isofocal dose and its impact on lithography[6].

Four resists were chosen for this simulation study: PBS, Nippon Zeon's ZEP 7000, Shipley's SPR 700 and a virtual "high gamma" resist. The first three were chosen because they are used at Etec, are commercially available, and have been tested for their dissolution rates using the ProDRM software package developed by FINLE Technologies. A "high gamma" or theoretical resist is included to determine the effect a "near-perfect" resist has on the lithographic response of an e-beam system when GHOST exposure is used. Table 1 lists the dissolution parameters for the four resists using the standard Mack model of resist development[7].

Table 1. Dissolution parameters.

Resist	R_{max} (nm/s)	R_{min} (nm/s)	m_{th}	n
PBS	32.9	2.23	-10.0	2.22
ZEP 7000	13.1	0.18	0.45	7.27
SPR 700	2.88	0.27	0.55	7.15
High gamma	100	0.50	0.50	50.0

Figure 2 is a plot of the dissolution responses for the four resists. The develop rate is plotted versus the fraction of resist not converted to the soluble form. As both Table 1 and Figure 2 show, there is a wide range of resist responses. The most important metrics of the resist response are the dissolution selectivity parameter n, which is proportional to resist contrast, and the ratio of the maximum to minimum development rates (R_{max}/R_{min}). The high gamma resist is close to infinite contrast and has a high dissolution ratio, transmitting the image of the exposure into the resist with little or no loss of fidelity. PBS, on the other hand, shows both a low contrast and a low dissolution rate ratio and will respond to a given exposure image quite differently. SPR 700 and ZEP 7000 exhibit relatively high contrast (intermediate between PBS and the high gamma resist), but have very different development ratios.

These dissolution rate parameters are specific to a 10 keV exposure and may not be generally applicable to other exposure energies. Also, the etch properties of the resist (whether a wet or dry etch is required, as well as the magnitude of any etch bias that occurs when manufacturing a mask) have not been accounted for. The amount of etch bias needed influences the optimal amount of lithographic bias that is selected and is not considered here. We know from previous work that the quality of the dry etch step is critical in maskmaking lithographic performance.

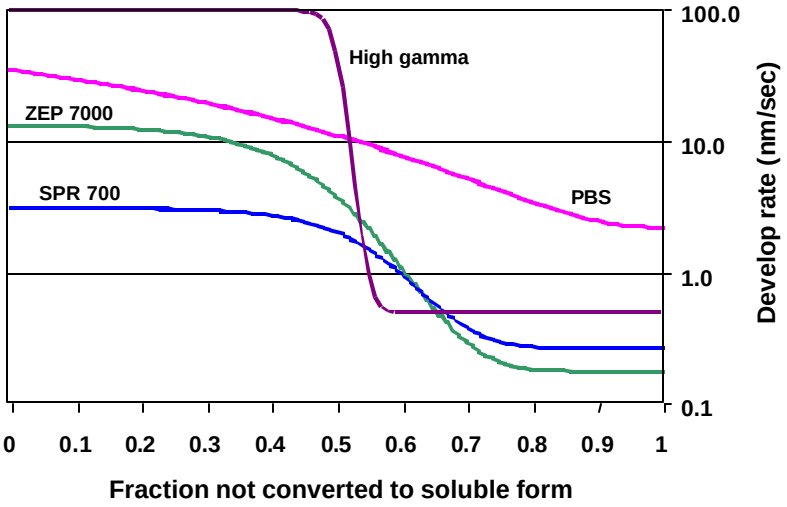

Figure 2. Semilog plot of develop rate versus unexposed resist fraction for four resists.

4. Theory of Raster Scan Imaging

Raster scan imaging can be thought of as the formation of an image by the summation of many spatially distinct basis images of (possibly) differing energies. In practice, this summation is always "incoherent", meaning the energy deposited into the resist material for each basis image is added together to form the total energy of the total image. A basis image, for example, could be simply the intensity of the spot of a laser beam as it is projected onto the surface of a substrate (or more correctly, deposited into a photoresist film). For the simplest raster scan imaging scheme, only one basis image is used, a so-called *spot* or *pixel* image, and each basis image has equal energy. Ignoring, for the purposes of this discussion, the distribution of energy through the thickness of the resist film, the raster scan image $I(x,y)$ can be described as the summation of many spatially-shifted basis images.

$$I(x,y) = \sum_{i=1}^{N} P(x-x_i, y-y_i) \qquad (1)$$

where $P(x,y)$ is the image of a single pixel or spot, and the set of points (x_i,y_i) represent the centers of each pixel that are being summed to form the final image (i.e., the address grid).

For both laser beam and electron beam raster scan writing tools, the pixel image can be fairly approximated as a Gaussian beam. As a simple starting place, let us assume that the only basis image being used is a symmetric Gaussian pixel. Normalizing the pixel to have a peak intensity of 1,

$$P(x,y) = \exp\left(-\frac{x^2+y^2}{2s^2}\right) = \exp\left(-\frac{x^2}{2s^2}\right)\exp\left(-\frac{y^2}{2s^2}\right) \qquad (2)$$

where the width of the Gaussian is defined by σ. Assume that the raster scan strategy being employed uses a fixed address grid with grid spacings Δx and Δy. The image being produced is then given by equation (1) with address grid points turned either on or off.

Two very simple examples will illustrate the formation of a raster scan image – an isolated spot and a large edge.

4.1 Image of a Single Spot

First, consider the simplest image – a single spot. In this case, only one address grid is "on" so that the total image is just

$$I_{spot}(x,y) = \exp\left(-\frac{x^2+y^2}{2s^2}\right) \tag{3}$$

Note that this is also the general result of the image in the vicinity of $x = y = 0$ whenever Δx and Δy are much greater than σ.

Using this simple result, we can derive some of the basic lithographic properties of the image. First, where is the "edge" of the image? In other words, when this image is printed in resist, where will the edges of the resist lie? Although this is a rather complicated question, it can be simplified by assuming the response of the resist to a Gaussian-shaped image is such that the resist edge will occur at an normalized energy threshold of I_{th}. For example, picking $I_{th} = 0.5$ would produces edges corresponding to the full width half maximum (FWHM) point of the image. In optical lithography, it has been shown empirically that most resists have near optimum performance when $I_{th} \approx 0.3$. For an arbitrary threshold intensity, the position of the left edge (at $y = 0$) is given by

$$x_{edge} = -s\sqrt{2\ln(1/I_{th})} \tag{4}$$

where the center of the spot is at x = 0. As an example, the FWHM ($I_{th} = 0.5$) width (= $2\,|x_{edge}|$) is equal to 2.355σ.

For the image of a spot, what is the quality of the image? One of the most useful metrics of image quality is the image log-slope: the slope of the logarithm of the image at the nominal photoresist edge. For the Gaussian spot image, the image log-slope is just

$$log-slope = \left.\frac{d\ln I}{dx}\right|_{x_{edge}} = \frac{\sqrt{2\ln(1/I_{th})}}{s} \tag{5}$$

It is quite apparent that equation (5) predicts improved image quality (improved log-slope) for a smaller spot beam (i.e., smaller σ). The image log-slope can be normalized by multiplying by the desired feature width to give the dimensionless normalized image log-slope (NILS). For this case, the NILS becomes

$$NILS = 4\ln(1/I_{th}) \tag{6}$$

If $I_{th} = 0.5$ the NILS will have a value of about 2.8. For $I_{th} = 0.3$ the NILS will become about 4.8. This increasing NILS with lower threshold intensity means that resist images printed at these lower threshold intensities will have much greater linewidth control. This higher NILS for a lower I_{th} means that the resist has a tendency to provide more stable images at lower threshold values (such as 0.3) rather than at higher threshold values (such as 0.5).

4.2 Image of an Edge

A second, somewhat less trivial, example is the image of an edge where all pixels such that $x_i \geq 0$ are turned on.

$$I_{edge}(x,y) = A(y)\sum_{n=0}^{\infty}\exp\left(-\frac{(x-n\Delta x)^2}{2s^2}\right) \tag{7}$$

where *A(y)* is the result of summing all pixels in the y-direction. An interesting special case occurs when the address grid becomes infinitely small. For such a case, the summation in equation (7) becomes an integral, *A(y)* becomes a constant, and an "ideal edge" image can be formed:

$$I_{ideal-edge}(x,y) = \frac{1}{\sqrt{2p}\,s}\int_{0}^{\infty}\exp\left(-\frac{(x-t)^2}{2s^2}\right)dt = \frac{1}{2}\mathrm{erfc}\left(-\frac{x}{\sqrt{2}\,s}\right) \tag{8}$$

where the image has been normalized to have a peak value of 1 and erfc(z) is the complimentary error function. Note that this image is "ideal" only in the sense that it is a limiting behavior and, in fact, may not be the best image for a particular application.

Where is the edge for this image of an edge? For two cases, $\Delta x >> \sigma$ and $\Delta x << \sigma$, the result can be determined analytically. When the address grid is much bigger than the Gaussian spot size, the edge position is just given by equation (4) since the edge is influenced almost exclusively by the nearest spot. When the address grid is much smaller than the spot size (a more common case), a simple result is also possible. Consider first the limiting case of an infinitely small address grid. Picking a specific threshold intensity, equation (8) can be solved for the position of the edge.

$$\begin{aligned} For\ I_{th} = 0.3, \quad x_{edge} &\approx -0.523\,s \\ For\ I_{th} = 0.5, \quad x_{edge} &= 0 \end{aligned} \tag{9}$$

When the address grid size Δx is bigger than zero, but still much smaller than the spot size, the edge position becomes

$$\begin{aligned} For\ I_{th} = 0.3, \quad x_{edge} &\approx -0.523\,s - \Delta x/2 \\ For\ I_{th} = 0.5, \quad x_{edge} &= -\Delta x/2 \end{aligned} \tag{10}$$

The position of the edge is extremely important, since obviously we want it to occur at its designed location (x = 0 in this case). Offsets from this desired position can be accommodated using data biasing.

The image quality of the raster scan printed edge can again be described by the image log-slope. Defining the log-slope at the edge position given by equation (10), the two cases are again $\Delta x >> \sigma$ and $\Delta x << \sigma$. If the address grid is much larger than the spot size, the image log-slope is given by equation (5), the log-slope of a single spot. When the address grid is much smaller than the spot size, equation (8) can be used to derive the log-slope.

$$\begin{aligned} For\ I_{th} = 0.3, \quad log-slope &\approx \frac{1.16}{s} \\ For\ I_{th} = 0.5, \quad log-slope &= \frac{\sqrt{2/p}}{s} \approx \frac{0.798}{s} \end{aligned} \tag{11}$$

As in the case of a single spot, both a smaller spot size and a lower I_{th} results in a better quality image of the edge.

The limiting cases discussed above provide analytic solutions to the position of the edge (relative to the position of the center of the first spot) and the log-slope of the image at the edge. Numerical evaluation of equation (7) can provide more general solutions. Figure 3 shows two examples of calculated images of an edge for different spot sizes. From these images, the edge positions and image log-slopes can also be calculated. Figures 4 and 5 show the results for different address grids and spot sizes assuming both I_{th} = 0.3 and I_{th} = 0.5. It is apparent that the behavior of a single spot and the behavior of the ideal edge (address grid = 0) provide an envelope for the imaging behavior. Further, the single spot limiting case is an accurate approximation to the real case when the address grid is bigger than about 1.2 times the spot size. The ideal edge limiting case is accurate when the spot size is greater than about twice the address grid. To be more specific, for the case when the spot size is equal to twice the address grid, equation (10) predicts the position of the edge accurately to within 3%.

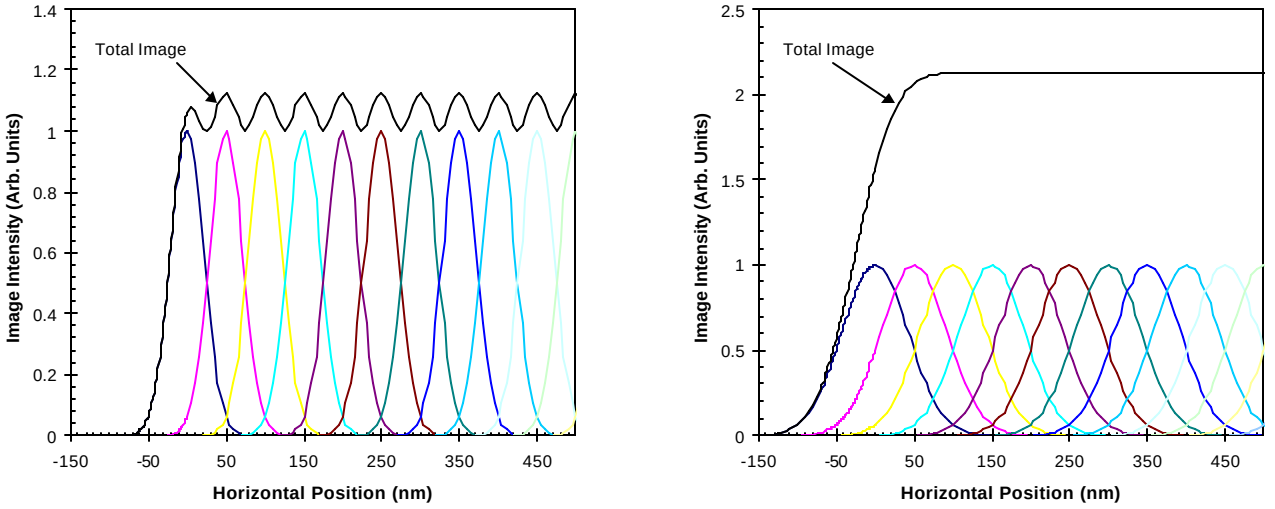

(a) (b)

Figure 3. The image of an edge calculated as the sum of many Gaussian spots for an address grid of 50nm and spots size of (a) 50nm, and (b) 100nm.

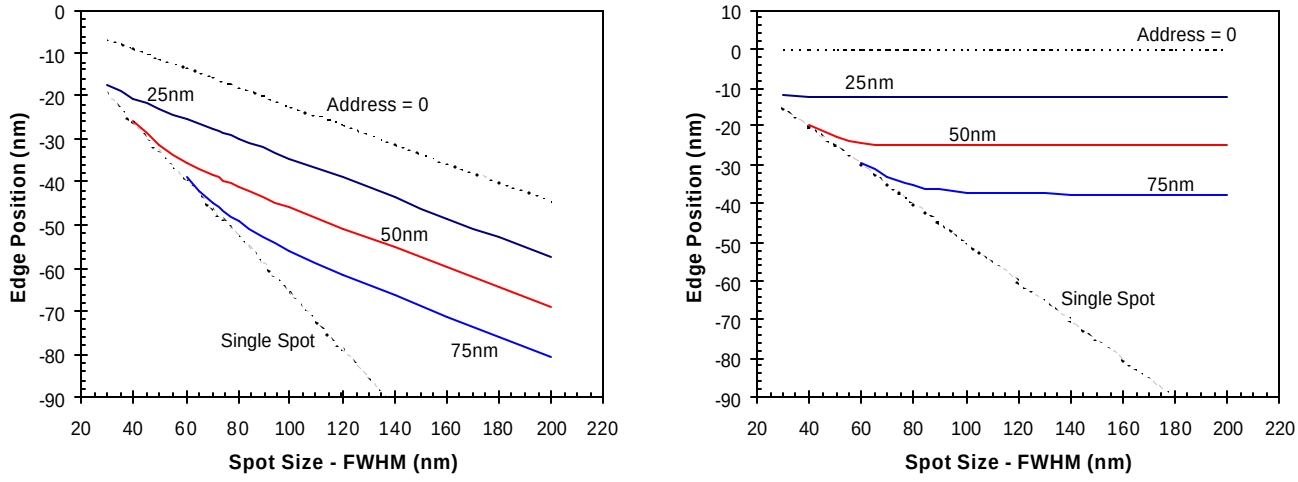

(a) (b)

Figure 4. The effects of spot size (for different address grid sizes) on the position of the edge of an edge image assuming the edge occurs at (a) I_{th} = 0.3, and (b) I_{th} = 0.5. The limiting cases of a single spot (address grid = ∞) and address grid equal to zero are shown as dotted lines.

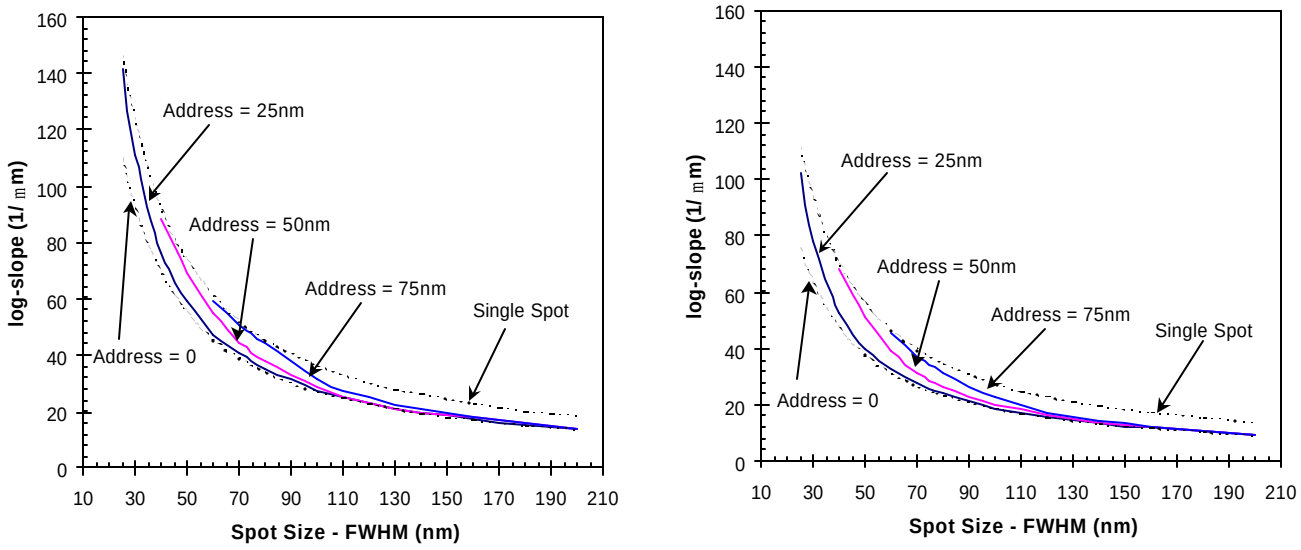

Figure 5. The effects of spot size (for different address grid sizes) on the image log-slope of an edge image assuming the edge occurs at (a) I_{th} = 0.3, and (b) I_{th} = 0.5. The limiting cases of a single spot (address grid = ∞) and address grid equal to zero are shown as dotted lines.

4.3 Effects of E-Beam Backscattering

The above discussion of the nature of raster scan imaging assumed a simple Gaussian basis function. For electron beam writing, scattering within the resist and the substrate can lead to an energy distribution in the resist that is more complicated than a simple Gaussian. Many authors have noted that this backscattering of electrons leads to a distribution that can be reasonably approximated by a double Gaussian. In one dimension, this could take the form

$$P(x) = (1-b)\exp\left(-\frac{x^2}{2s^2}\right) + b\exp\left(-\frac{x^2}{2s_B^2}\right) \qquad (12)$$

where σ_B defines the width of the backscatter component of the distribution ($\sigma_B > \sigma$) and β describes its strength (roughly equivalent to the fraction of electrons that are backscattered).

Consider an edge made of the summation of these double Gaussian spots. For the ideal edge case (infinitely small address grid), the edge becomes the sum of two complimentary error functions:

$$I_{ideal-edge}(x) = \frac{1}{2}\left[(1-b')\mathrm{erfc}\left(-\frac{x}{\sqrt{2}s}\right) + b'\mathrm{erfc}\left(-\frac{x}{\sqrt{2}s_B}\right)\right] \qquad (13)$$

where $$b' = \frac{b s_B}{(1-b)s + b s_B}$$

The impact of this scattering on the log-slope of the image at the edge is given by

$$For\ I_{th} = 0.5, \quad log-slope = \sqrt{\frac{2}{p}}\left(\frac{1-b'}{s} + \frac{b'}{s_B}\right) \tag{14}$$

It is clear from this equation that both larger β' and larger σ_B result in a lower log-slope. As an example, 10 keV exposure of 400nm thick resist on a mask blank with a 220nm FWHM spot would typically produce $\sigma \approx 100$nm, $\sigma_B \approx 400$nm, and $\beta \approx 0.1$ (as calculated with ProBEAM/3D). This would give a $\beta' \approx 0.308$. The log-slope in this case is about 23% lower than if there had been no scattering.

4.4 The Effects of Ghost Exposure

Ghost exposure is a means to correct for the varying affects of backscattering as a function of pattern density. This is accomplished by subjecting the resist to a second exposure (after the normal writing of the pattern) comprised of a negative of the original pattern, exposed using a large spot and with a dose smaller than the original. In other words, the goal of the ghost exposure is to mimic the backscattered portion of the exposure in the nominally unexposed areas, thus equaling out the impact of this unwanted effect. For example, the ghost correction pattern for the isolated edge of equation (13) would be an opposite-facing edge with lower energy:

$$I_{ghost-edge}(x) = \frac{a}{2}\left[(1-b'_g)\mathrm{erfc}\left(+\frac{x}{\sqrt{2}s_g}\right) + b'_g\,\mathrm{erfc}\left(+\frac{x}{\sqrt{2}s_B}\right)\right] \tag{15}$$

where σ_g is the width of the ghost exposure spot and α is the ghost dose relative to the normal exposure dose. If the ghost spot width is adjusted to equal the backscatter Gaussian width (i.e., $\sigma_g = \sigma_B$), the ghost edge simplifies to

$$I_{ghost-edge}(x) = \frac{a}{2}\mathrm{erfc}\left(+\frac{x}{\sqrt{2}s_B}\right) \tag{16}$$

Adding the ghost pattern to the original exposure of equation (13),

$$I_{total-edge}(x) = \frac{1}{2}\left[(1-b')\mathrm{erfc}\left(-\frac{x}{\sqrt{2}s}\right) + b'\mathrm{erfc}\left(-\frac{x}{\sqrt{2}s_B}\right)\right] + \frac{a}{2}\mathrm{erfc}\left(+\frac{x}{\sqrt{2}s_B}\right) \tag{17}$$

By letting $\alpha = \beta'$, an interesting result occurs: the backscattered pattern becomes a simple, uniform background dose.

$$I_{total-edge}(x) = \frac{1}{2}\left[(1-b')\mathrm{erfc}\left(-\frac{x}{\sqrt{2}s}\right)\right] + b' \tag{18}$$

The result of this "optimized" GHOST pattern is to eliminate the backscattered spatial distribution of energy and replace it with a constant background dose, independent of the proximity of other features.

The impact of this optimized ghost pattern on the log-slope of the edge can now be determined.

$$For\ x_{edge} = 0, \quad log - slope = \sqrt{\frac{2}{p}}\left(\frac{1-b'}{1+b'}\right)\left(\frac{1}{s}\right) \tag{19}$$

Thus, ghosting reduces the log-slope even further. For the case described previously ($\sigma_B \approx 4*\sigma$, and $\beta = 0.1$), the log-slope is decreased by 31% compared to the no-ghost case. About two-thirds of this decrease in log-slope is due to the higher relative energy level of the image at the edge. Figure 4 shows how the ghost proximity correction scheme affects this image of an edge.

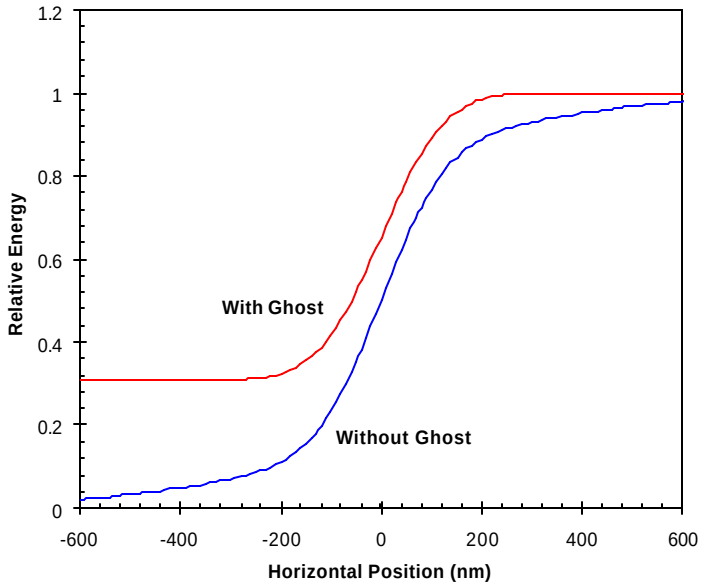

Figure 6. The impact of an optimized ghost exposure on an ideal edge (with σ = 100m, $\sigma_B \approx$ 400nm, and β = 0.1).

5. Optimization of Lithography — Design of Experiments (DOE) of Simulation Data

5.1 Description

Estimates of the critical dimension (CD) performance of a typical mask writing application were made by modeling resist responses at various conditions of dose, develop time, data bias, and spot size. All models used 10 keV energy, multipass gray (MPG) writing strategy[3] and the GHOST correction strategy, a 25 nm input address, a 400 nm resist thickness, and 700 nm isolated clear tone features. The isolated space (clear) feature was chosen as the worst case example of how GHOST affects process latitude. For simplification, the same MPG edge formation (all spots lined up on the edge) was used for all feature simulations. The GHOST exposure used for all

simulations employed a ratio of GHOST to primary dose (Q_c/Q_p) of 0.4125 with a FWHM spot size of 1150 nm ($\sigma_g \approx$ 500nm). To accomplish this in ProBEAM/3D, the multiple exposure mode was used with the primary exposure first and the GHOST exposure added as a second exposure. The summed exposure image was then run through the development model and the resist profile was measured. The resist CD was simulated under these conditions using ProBEAM/3D version 5.1q. A 2-D slice was made in each trial, and measurements of the CD were made using the weighted threshold model at a 10% level (resist height from the bottom of the resist). A four-variable, three-level, full-factorial design was chosen. The variables included exposure dose (±20%), development time (±50%), FWHM spot size (100 to 300 nm), and data bias (0 to -200 nm). The number of trials for each resist tested was 81. The resist thickness used for the GHOST exposures was set at 100 nm thicker than the non-GHOST case due to the higher resist loss with GHOST.

Table 2 lists the variables tested. The responses examined were CD and exposure latitude, represented as ΔCD/Δ%dose. The response ΔCD/Δ%dose can be easily determined by simulation and is a key parameter in designing lithography tools. The response of PBS to GHOST exposures was so poor that it was impossible to find a usable process window under any conditions. As a consequence, no results for PBS are available.

Table 2. Conditions for lithography optimization using DOE.

Resist	**Dose** ($\mu C/cm^2$)	**Develop Time** (sec)	**Spot Size** (nm)	**Data Bias** (nm)
PBS	2, 2.5, 3	30, 60, 90	100, 200, 300	0, -100, -200
ZEP 7000	8, 10, 12	100, 150, 200	100, 200, 300	0, -100, -200
SPR 700	8, 10, 12	250, 325, 400	100, 200, 300	0, -100, -200
High gamma	2, 2.5, 3	30, 60, 90	100, 200, 300	0, -100, -200

The data from each resist was fit to either a linear or quadratic response function using the DOE software package Stat Expert. Separate solutions to both CD and ΔCD/Δ%dose were derived. Figures 7 to 10 are examples of some of the plots generated, showing both GHOST and non-GHOSTED results for comparison.

5.2 Comparison of Resist Responses

Figures 7 and 8 are comparisons of CD and ΔCD/Δ%dose responses for a GHOST and non-GHOST exposure for ZEP 7000. As the plots show, the contour intervals for the non-GHOST exposure are wider, indicating greater process latitude. Of interest are the values for ΔCD/Δ%dose for the two exposure types. Assuming a desired CD control threshold of 10 nm/%dose or less, there is substantially less area for an acceptable range for the GHOST exposure compared to the non-GHOST exposure. In particular, GHOST reduces the exposure latitude at nominal and over-exposure conditions relative to the non-GHOST case. One important thing to note from these plots of ZEP 7000 is that both types of exposures have a reasonable process solution.

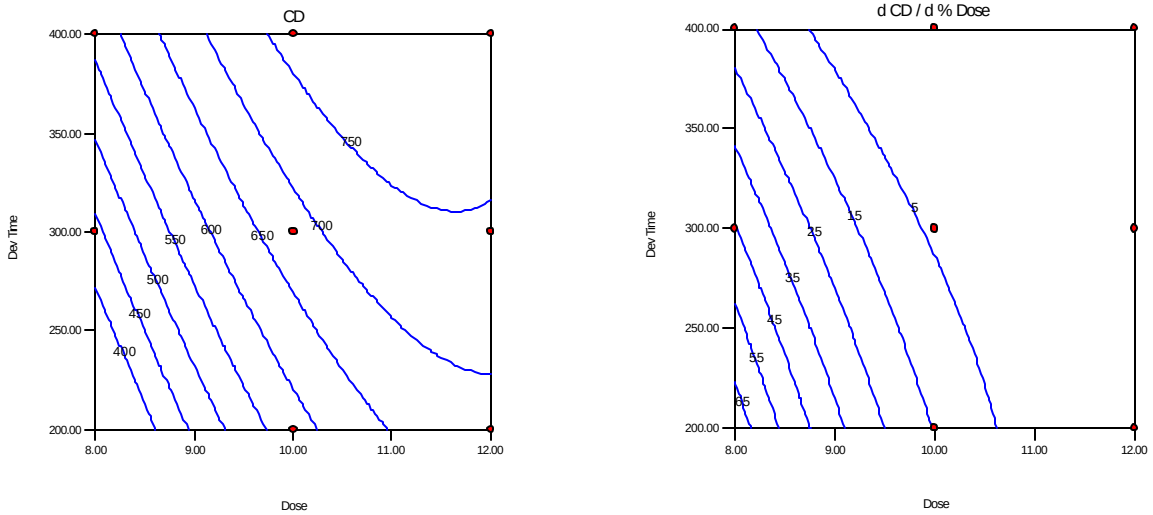

(a) (b)

Figure 7. Contour plots of (a) CD and (b) ΔCD/Δ%dose for 300 nm thick ZEP 7000 with no GHOST as a function of dose and develop time (100 nm spot size and -100 nm bias).

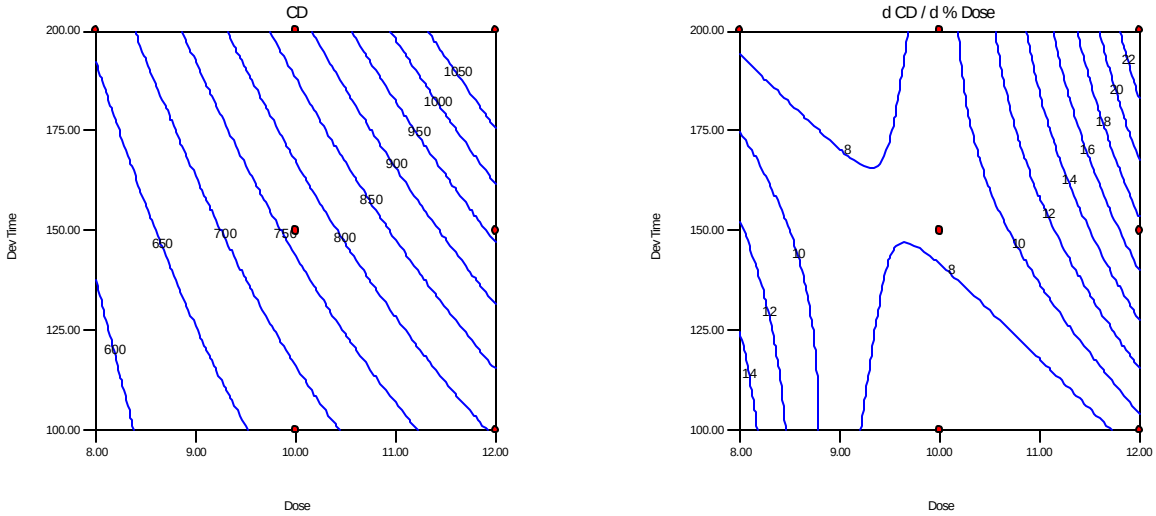

(a) (b)

Figure 8. Contour plots of (a) CD and (b) ΔCD/Δ%dose for 400 nm thick ZEP 7000 with GHOST as a function of dose and develop time (100 nm spot size and -100 nm bias).

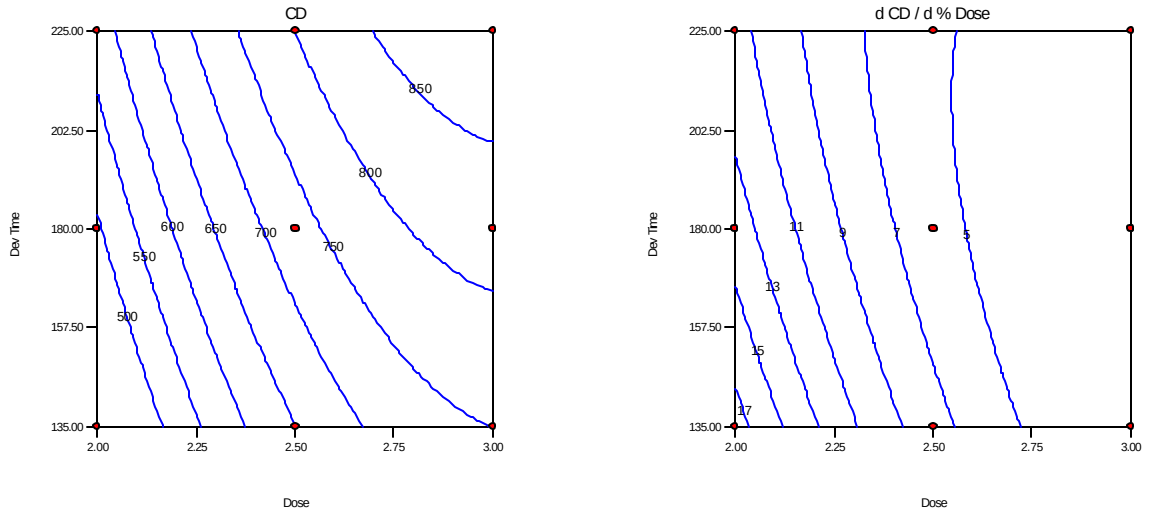

(a) (b)

Figure 9. Contour plots of (a) CD and (b) ΔCD/Δ%dose for 300 nm thick high gamma resist with no GHOST as a function of dose and develop time (100 nm spot size and -100 nm bias).

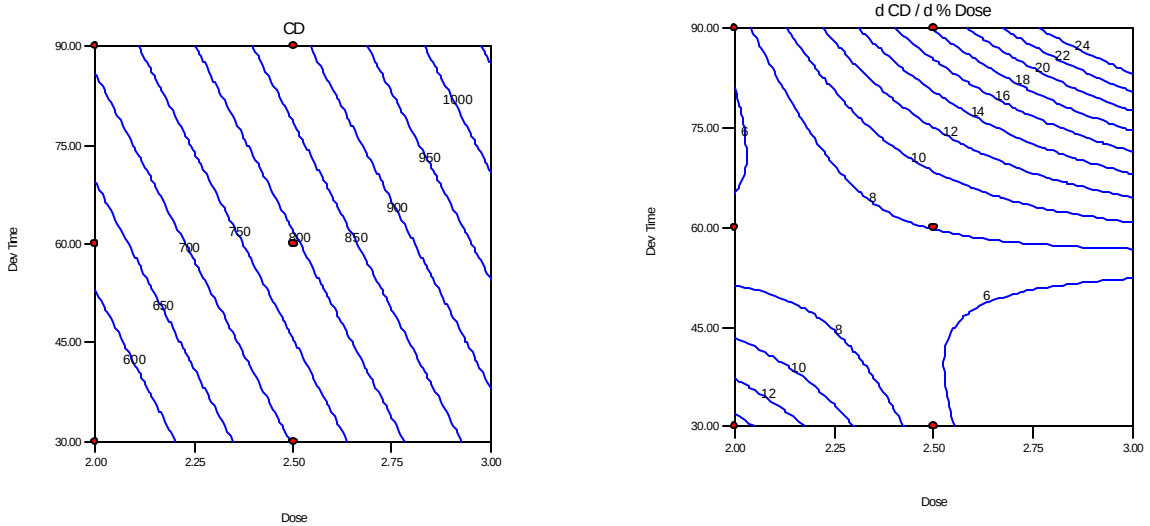

(a) (b)

Figure 10. Contour plots of (a) CD and (b) ΔCD/Δ%dose for 400 nm thick high gamma resist with GHOST as a function of dose and develop time (100 nm spot size and -100 nm bias).

Figures 9 and 10 are similar plots for the high gamma resist. While the acceptable amount of factor space (the area that has an acceptable solution) is similar for the two resists, there is a significant difference in the ΔCD/Δ%dose. The high gamma resist has a much greater latitude. The benefits of using a higher resist contrast can be seen by comparing the ΔCD/Δ%dose of Figures 7 to 9. The high gamma resist tends to have improved under-exposure latitude. What is not shown in these plots is the fact that the high gamma resist exhibits sever undercutting (worse at high doses) due to the forward scattering inherent in 10 keV exposures.

5.3 Determination of Process Latitude

To find an optimum latitude for the process, it is instructive to overlay the plots for CD and ΔCD/Δ%dose and find process conditions of simultaneous solutions for both responses. Figures 11 and 12 are overlay plots of the two responses, using specifications of 670–730 nm CD and a ΔCD/Δ%dose of 0–10nm/%. The white area on the graph represents the regions where both conditions are simultaneously satisfied. The CD constraints may be considered as the boundary conditions for a test of acceptable ΔCD/Δ%dose. This is a graphical way to define process latitude for a series of exposures, develop times, spot sizes, and data bias conditions[5].

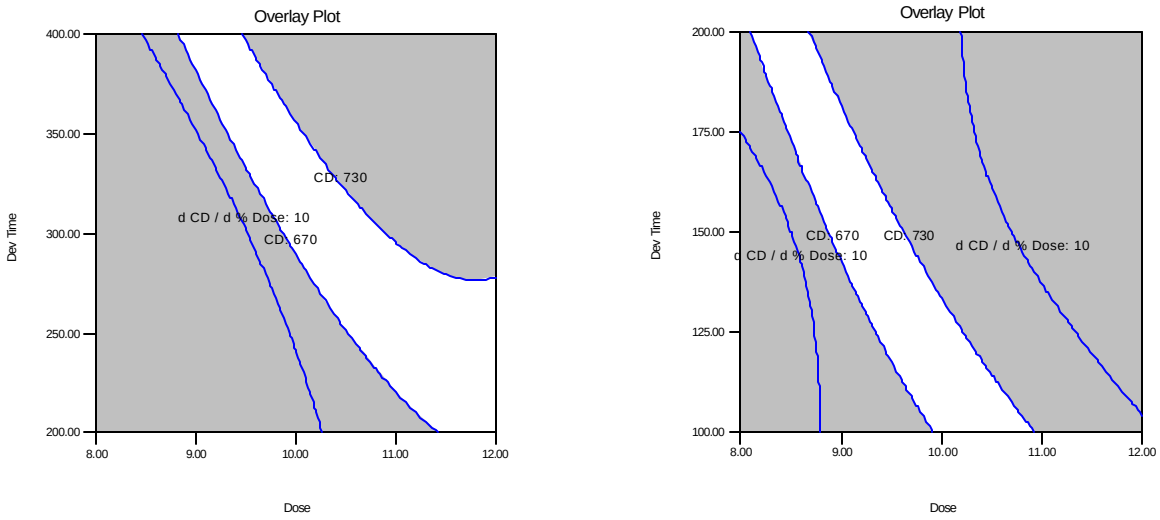

Figure 11. Overlay plots for (a) 300 nm thick ZEP 7000 with no GHOST and (b) 400 nm thick ZEP 7000 with GHOST as a function of dose and develop time (100 nm spot size and -100 nm bias).

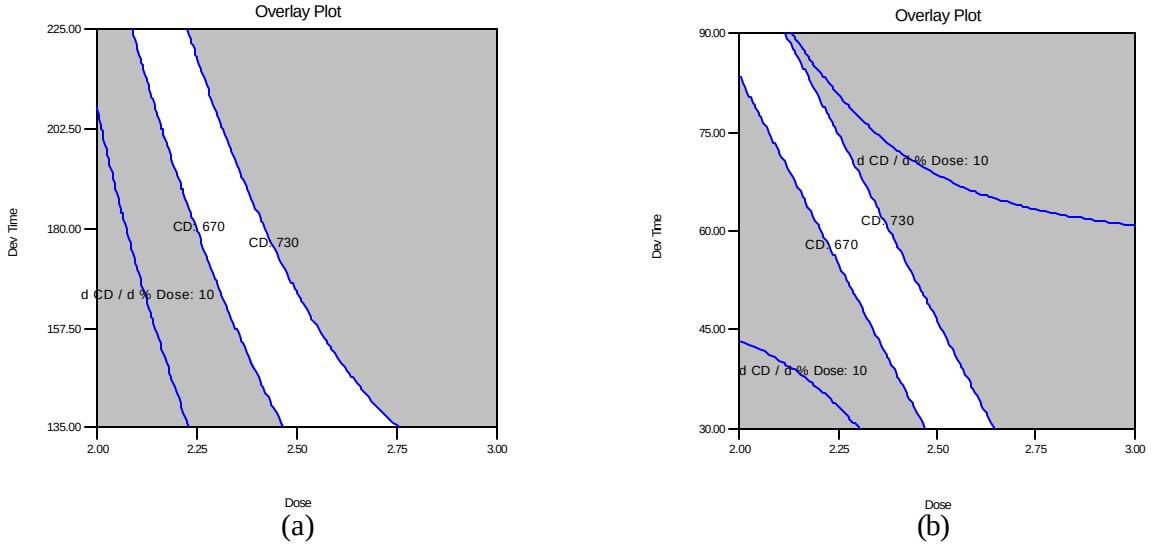

Figure 12. Overlay plots (process windows) for (a) 300 nm thick high gamma resist with no GHOST and (b) 400 nm thick high gamma resist with GHOST as a function of dose and develop time (100 nm spot size and -100 nm bias).

A comparison of Figures 11 and 12 is instructive. For both resists, the ability of GHOST to provide a reasonable process solution is reduced compared to non-GHOSTED lithography. Surprisingly, the latitude of the high gamma resist does not show a performance benefit. This is may be due to the undercutting exhibited in the resist profiles.

Appendices A–C provide plots of simultaneous optimization analysis for each of four resists. The plots include three spot sizes and three data sizing conditions. Appendix A contains plots for ZEP 7000. The effect of increasing data bias is to shift the acceptable process window towards a greater range of acceptable doses. As the data bias increases, the acceptable process window increases. Responses for ZEP 7000 indicate that the resist response to these conditions is robust. Larger spot sizes result in a decreased process window. Appendix B contains plots for SPR 700. As with the ZEP 7000 plots, data bias also shifts the acceptable window towards a higher range of doses, and the effect of increased data bias is to increase the process window. Also note that the process windows for SPR 700 are smaller than for ZEP 7000, indicating that the development discrimination ratio R_{max}/R_{min} has a noticeable impact on resist performance. Appendix C contains plots for the high gamma resist. These plots describe the limit for 10 keV lithography with the combination of writing strategy, spot sizes, and input addresses studied. Results show clearly that bias is a key parameter for optimizing CD performance. Data bias has a very large impact on process latitude, with an optimum data bias improving process latitude. Spot sizes of 200 and 300 nm had no solution.

6. Conclusions

Results from simulations indicate that a noticeable loss of process latitude is an unavoidable side effect of using the GHOST writing strategy. Work with a simple, analytical image model of an edge indicates that a degradation of ~30% in exposure latitude is expected with the use of GHOST at typical 10 keV conditions. While the latitude is reduced, sufficient process latitude still remains to have a viable process. All of the GHOST processes tested here work best with small (i.e., ~100 nm) spot sizes. Running with spot sizes at or below 100 nm is a key component in making these systems work with sufficient CD control. An increase in data bias also has the effect of increasing the process latitude to a point, after which further increases reduce process latitude. As with all of this simulation work, the results are conservative because the effect of dry etch on the profiles is not accounted for. Results from the PBS simulations were unacceptable because of the poor contrast and so were not included in the results. Most of the profiles for the high gamma resist exhibited a retrograde (i.e., $> 90^{o}$ profile).

7. Future Work

Future work is planned on exploring optimal dissolution parameters in more detail. Simulations with the high gamma resist parameters clearly indicate that the combination of the spatial energy distribution caused by the physics of electron scattering and the dissolution response to this energy distribution results in a complicated lithographic system that must be optimized as a system. In particular, the work done in preparation for this paper indicates that matching the properties of high contrast chemically amplified resists with 10 keV scattering is a key part of performance optimization. Using simulation to determine optimal resist parameters and then fine tuning a process to achieve these parameters could be an effective approach towards process development.

8. Acknowledgements

Thanks to David Alexander for his work on dissolution rate parameters.

9. Trademarks

Appendix A. Operating Characteristic Overlay Plot for ZEP 7000

Overlay process window plots for ZEP 7000 using the standard GHOST process (Q_c/Q_p = 0.4125, 1150 nm GHOST spot, 700 nm clear features, MPG, 25 nm input address), for different spot sizes and data biases. The CD specification was set to the range of 670–730 nm, and the acceptable ΔCD/Δ%dose range was 0–10 nm/%.

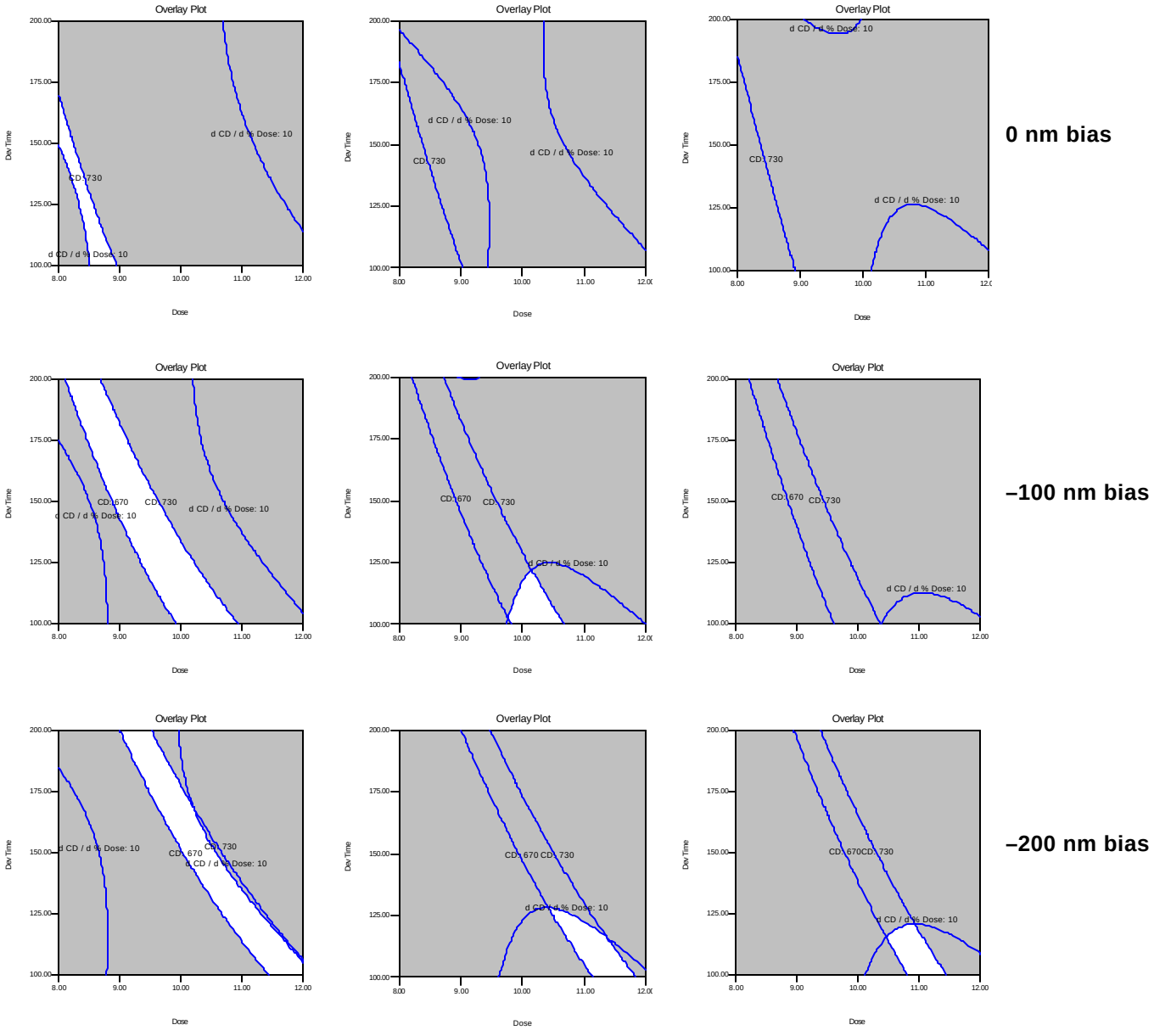

Appendix B. Operating Characteristic Overlay Plot for SPR 700

Overlay process window plots for SPR 700 using the standard GHOST process (Q_c/Q_p = 0.4125, 1150 nm GHOST spot, 700 nm clear features, MPG, 25 nm input address), for different spot sizes and data biases. The CD specification was set to the range of 670–730 nm, and the acceptable ΔCD/Δ%dose range was 0–10 nm/%.

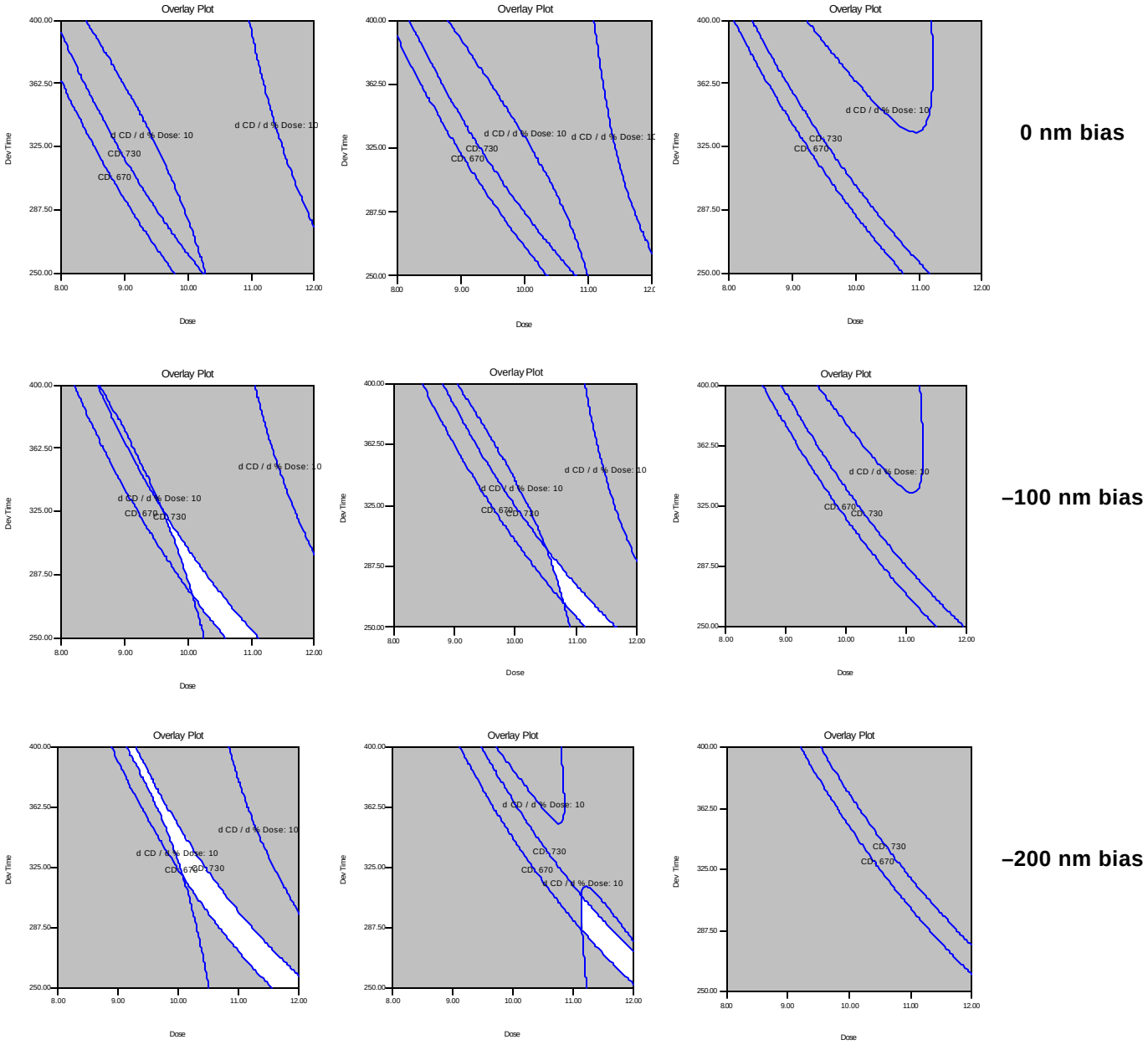

Appendix C. Operating Characteristic Overlay Plot for the High Gamma Resist

Overlay process window plots for the high gamma resist using the standard GHOST process (Q_c/Q_p = 0.4125, 1150 nm GHOST spot, 700 nm clear features, MPG, 25 nm input address), for different spot sizes and data biases. The CD specification was set to the range of 670–730 nm, and the acceptable ΔCD/Δ%dose range was 0–10 nm/%.

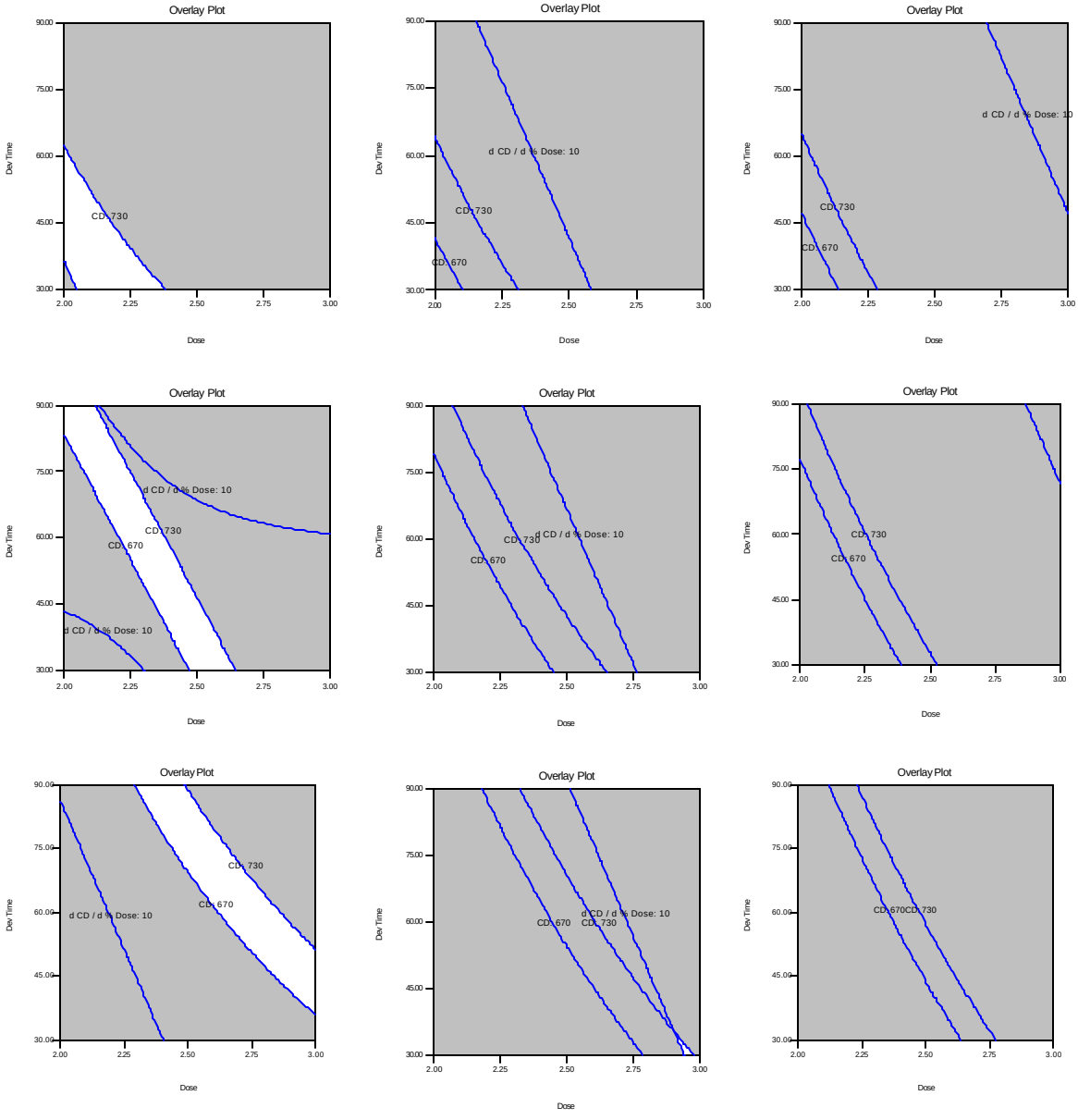

10. References

[1] G. Owen and P. Rissman, "Proximity effect correction for electron beam lithography by equalization of background dose:, *J. App. Physics*, Vol. 54, No. 6, pp. 3573-81 (1983).

[2] K. Ozawa, N. Abe, "Puddle developers for ZEP7000", *19th Annual BACUS Symposium on Photomask Technology and Management*, this conference.

[3] M. Lu, T. Coleman, and C. Sauer, "A 180-nm mask fabrication process using ZEP 7000, multipass gray, GHOST, and dry etch for MEBES 5000," *18th Annual BACUS Symposium on Photomask Technology and Management*, SPIE Vol. 3546, p. 98 (1998).

[4] C. Sauer, D. Alexander and C. Mack, "Electron-beam lithography simulation for mask making II. Comparison of the lithographic performance of PBS and EBR 900-M1," *17th annual BACUS Symposium of Photomask Technology and Management*, SPIE Vol. 3236, pp. 413-423 (1997).

[5] C. Mack, "Electron-beam lithography simulation for mask making: III. Effect of spot size, address grid, and raster writing strategies on lithographic performance with PBS and ZEP 7000," *18th Annual BACUS Symposium on Photomask Technology and Management*, SPIE Vol. 3546, pp. 32–44 (1998).

[6] C. Sauer, C. Mack, "Electron-beam lithography simulation for maskmaking, part IV: Effect of resist contrast on isofocal dose, " *Photomask Japan 1999*, to be published.

[7] C. A. Mack, Inside PROLITH, A Comprehensive Guide to Optical Lithography Simulation, FINLE Technologies (Austin, TX: 1997), pp. 106-110.